



UNIVERSITY OF LEEDS

This is a repository copy of *Linear and Helical Cesium Iodide Atomic Chains in Ultranarrow Single-Walled Carbon Nanotubes: Impact on Optical Properties*.

White Rose Research Online URL for this paper:
<https://eprints.whiterose.ac.uk/177967/>

Version: Supplemental Material

Article:

Kashtiban, RJ, Burdanova, MG, Vasylenko, A et al. (7 more authors) (2021) Linear and Helical Cesium Iodide Atomic Chains in Ultranarrow Single-Walled Carbon Nanotubes: Impact on Optical Properties. ACS Nano, 15 (8). acsnano.1c03705. pp. 13389-13398. ISSN 1936-0851

<https://doi.org/10.1021/acsnano.1c03705>

Reuse

Items deposited in White Rose Research Online are protected by copyright, with all rights reserved unless indicated otherwise. They may be downloaded and/or printed for private study, or other acts as permitted by national copyright laws. The publisher or other rights holders may allow further reproduction and re-use of the full text version. This is indicated by the licence information on the White Rose Research Online record for the item.

Takedown

If you consider content in White Rose Research Online to be in breach of UK law, please notify us by emailing eprints@whiterose.ac.uk including the URL of the record and the reason for the withdrawal request.



eprints@whiterose.ac.uk
<https://eprints.whiterose.ac.uk/>

Linear and Helical Cesium Iodide Atomic Chains in Ultra-Narrow Single Walled Carbon Nanotubes: Impact on Optical Properties – Supporting Information

Reza J. Kashtiban,^{1*} Maria G. Burdanova,¹ Andrij Vasylenko,^{1,2*} Jamie Wynn,³ Paulo V. C. Medeiros,³ Quentin Ramasse,^{4,5} Andrew J. Morris,⁶ David Quigley,¹ James Lloyd-Hughes¹ and Jeremy Sloan^{1*}

¹Department of Physics, University of Warwick, Coventry, CV4 7AL UK

²Department of Chemistry, University of Liverpool, Crown Street, Liverpool, L69 7ZD UK

³Cavendish Laboratory, University of Cambridge, Cambridge, CB3 0HE UK

⁴SuperSTEM Laboratory, SciTech Daresbury Campus, Daresbury, WA44AD UK

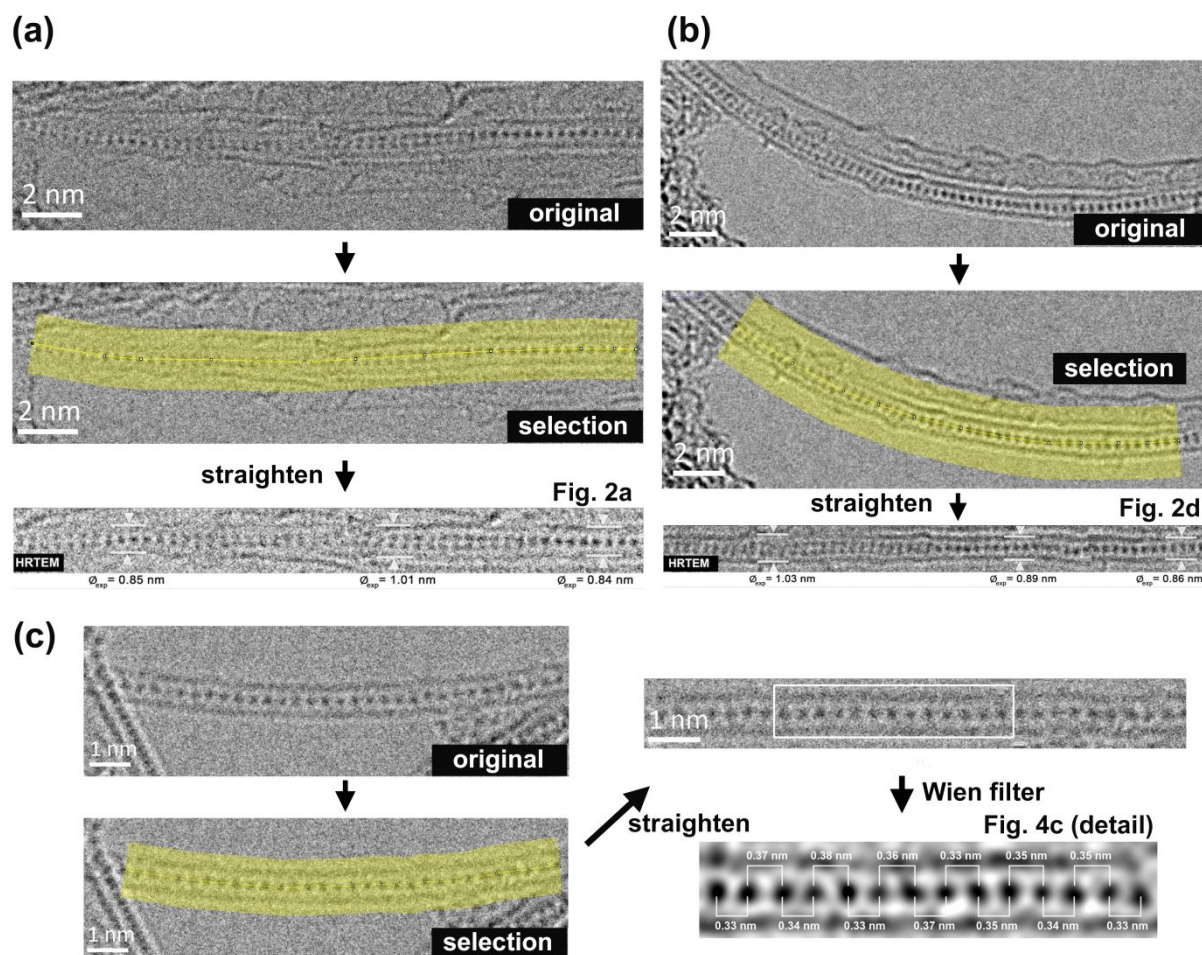
⁵School of Chemical and Process Engineering, University of Leeds, Leeds LS2 9JT, UK

⁶School of Metallurgy and Materials, University of Birmingham, Birmingham, B15 2TT UK

*Correspondence to: j.sloan@warwick.ac.uk, r.kashtiban@warwick.ac.uk, A.Vasylenko@liverpool.ac.uk

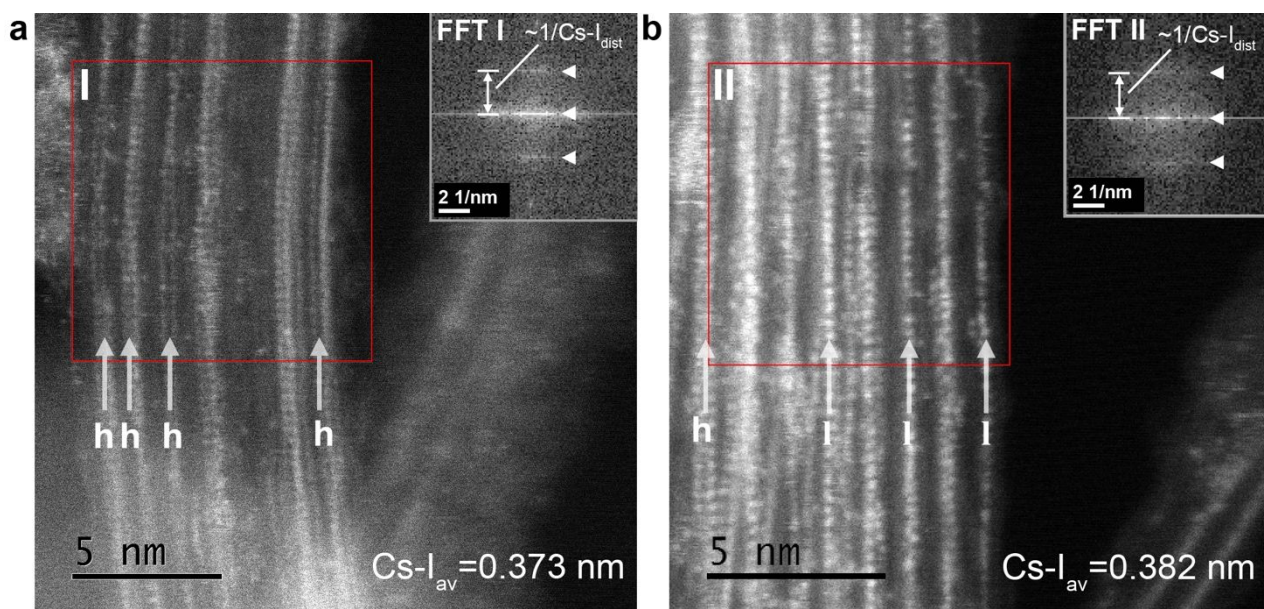
IMAGING AND IMAGE PROCESSING, ADDITIONAL IMAGES

Details of straightening procedures used on curved filled SWCNT images For aberration corrected High Resolution Transmission Electron Microscopy (HRTEM) and Annular Dark Field (ADF) single walled carbon nanotubes (SWCNTs) filled with helical 2×1 CsI and linear -I-Cs-I-Cs-I-1 linear chains, it is useful for the purposes of a closer comparison between crystals to straighten some of the images with negligible distortion. This is especially useful for helical 2×1 CsI crystals as it facilitates length measurements of their helical pitches but this approach was also used to straighten some linear CsI chains in addition. This procedure was applied to the HRTEM images of helical CsI chains in main article Figs. 1(c), (e) and (g), Figs. 2(a) and (b) and also to the linear CsI chain in Fig. 5(c), bottom detail. The straightening procedure was also applied to the ADF images in Fig. 2(g)I-IV and Fig. 5(c), bottom detail. The procedure for straightening the images in Figs. 2(a), 2(d) and 4(c) is outlined in Fig. S1 below, the steps being described in the caption.



Supporting Figure S1 This Figure explains the straightening and Wien filtering protocol used on helical 2×1 and True 1D atomic chains: (a, b) Straightening operations as performed on original images used to create Figs. 2(a) and 2(d) using the 'Straighten' protocol in ImageJ.^{S1} First a 200 long pixel selection is created from the original unprocessed image. Next the 'Straighten' command is applied to produce the final image without any further processing. On average, this protocol changes the Cs-I separations (the effect on the SWCNT diameter is negligible) by about 0.01%, well within experimental error. (c), as for (a) and (b) but this time a Wien filter is applied.^{S2}

Additional structure measurements from ADF images obtained from SWCNT bundles filled with CsI Average Cs-I separations (*i.e.* $Cs-I_{dist}$) can be measured from HRTEM or ADF STEM images of bundles of SWCNTs filled sometimes with predominantly helical CsI chains (denoted ‘h’) as shown here in Fig. S2(a) or more prominently with linear -I-Cs-I-Cs-I- chains (denoted ‘I’) as shown here in Fig. S2(a) from Fast Fourier Transforms obtained from the indicated 256×256 pixel regions I and II (*i.e.* FFT I and FFT II, respectively). The same FFT protocol is also applied to the measurement of I-I separations in iodine (I_x) linear chains in Fig. 5(d) and inset in the main article. The FFTs were generated using the appropriate function as supplied in Digital Micrograph GMS, version 3. The longitudinal Cs-I separations recorded in FFT I and FFT II are a convolution of the helical 2×1 or linear -I-Cs-I-Cs-I- chains with other Cs-I structures in the bundles and yield average real space Cs-I separations of 0.373 nm and 0.382 nm separations with approximate errors of ± 0.010 nm. This is good enough precision to distinguish CsI filling from pure iodine filling where the average I-I separation is 0.301 nm (Fig. 5(d), inset top).

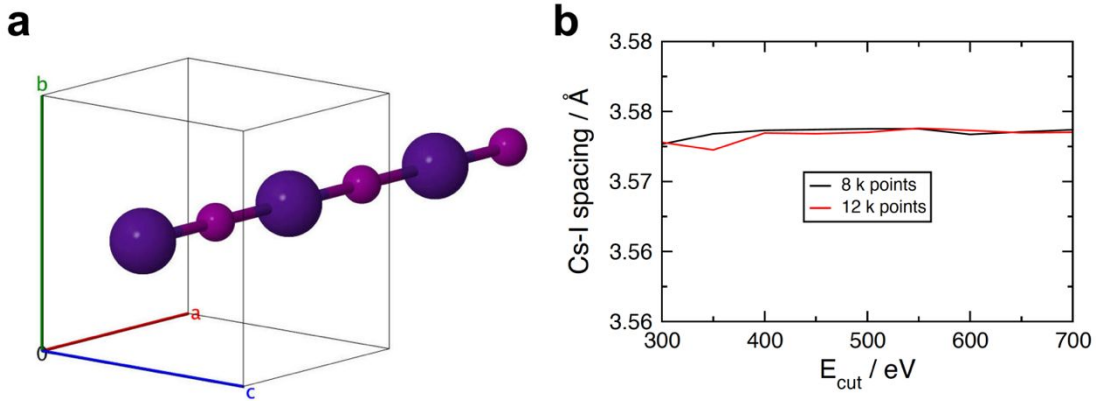


Supporting Figure S2 Here we demonstrate measuring average spacing of -Cs-I- using the Fast Fourier Transform (FFT) protocol.¹³ (a) ADF image and inset FFT obtained from the indicated red box (I) of an aligned curved bundle of SWCNTs containing both helical and single chain CsI. Obtained FFT indicates an average Cs-I spacing ($Cs-I_{av}$) of 0.373 nm. (b) ADF image and inset FFT obtained from the indicated red box (II) of second aligned and straighter bundle of SWCNTs containing mostly single chain CsI. The obtained FFT indicates an average Cs-I spacing ($Cs-I_{av}$) of 0.382 nm. These images also show the very high filling ratio of approaching 80-90% of all observed SWCNTs in some bundles although lower rates (*i.e.* 50-60%) were observed in other bundles.

MODELING CAESIUM IODIDE 1D WIRES AND SWCNT INTERACTIONS

Relaxed Ion Pair The Cs-I distance is calculated using Two-Point Steepest Descent TPSD geometry optimisation.^{S3} The model is based on a single ion pair in a box, periodic in the chain direction as shown in Fig. S3(a). Supercell is $8 \text{ \AA} \times 8 \text{ \AA}$ in the non-periodic direction. Checking convergence of Cs-I separation as a function of plane-wave cut-off energy (CASTEP, using the Perdew, Burke and Ernzerhof (PBE) functional, Refs. 36 and 37 main article) and k point sampling

density along the periodic direction. Calculations are already sufficiently converged for this purpose at 300 eV and 8 k points (4 under symmetry) for the single ion pair. The results are shown in Fig. S3(b).

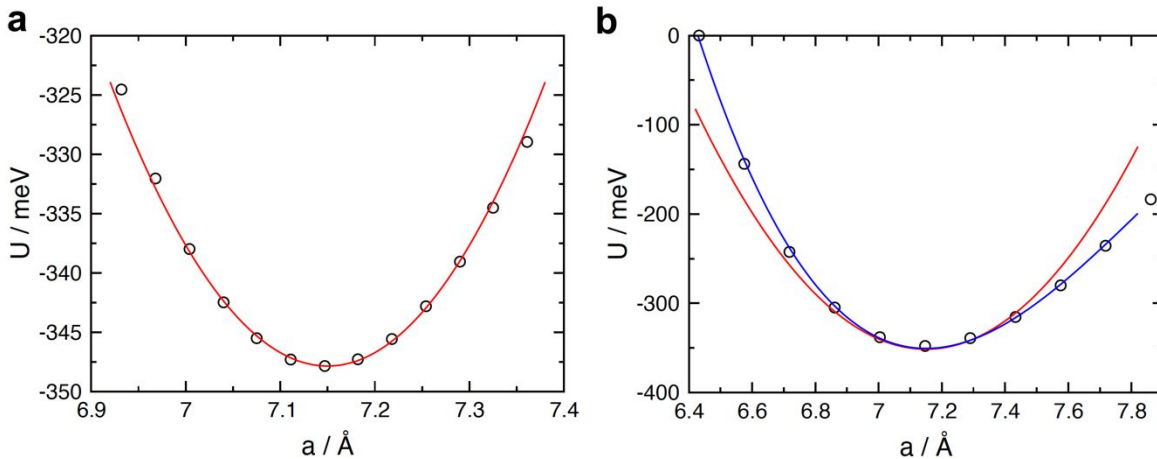


Supporting Figure S3 Computation of relaxed Cs-I spacing for an infinite periodic chain in a vacuum : (a) Shows the calculation geometry which consists of a unit cell containing two ions and which is periodic along the a-axis; (b) shows the convergence of vacuum Cs-I spacing with respect to the basis set size and k point sampling. In this and all subsequent models, the CsI models are represented with Cs = small light purple spheres and I = darker purple larger spheres.

Stretched ion pair The unit cell in the previous section has an equilibrium length of 7.14 Å and an equilibrium Cs-I spacing of 3.575 Å. If seeking to model this system as a 1D chain of atoms connected with simple harmonic springs, with equilibrium spacing l and spring constant k , the potential energy of the stretched unit cell containing two bonds should be

$$U = U_0 + 2 \times \frac{1}{2}k\left(\frac{a}{2} - l\right)^2 = U_0 + k\left(\frac{a}{2} - l\right)^2 \quad (1)$$

with $l = 3.575$ Å. The stretched unit cell parameter is a and U_0 a constant. Sampling of the a parameter performed with a fine (max $\delta l \pm 0.2$ Å) and coarse (max $\delta l \pm 0.6$ Å). Data and resulting fits are shown in Fig. S4(a,b). The purely harmonic fit to the fine data set results in $k = 1842$ meV/Å², with a maximum absolute error of 1.6 meV, and a mean absolute error of 0.43 meV. The fit can be significantly improved by ignoring the four most extreme data points, leading to $k = 1826$ meV/Å² with a maximum absolute error of 0.2 meV, and a mean absolute error of 0.13 meV, however this restricts bond stretches to ± 0.07 Å.



Supporting Figure S4 Calculation of Cs-I chain energetics under stretching/compression of single Cs-I unit cell : (a) Fine grained sampling of a (points) with harmonic fit (red); (b) Coarse grained sampling of a (points) with cubic fit (blue) and harmonic fit (red).

For the broader (coarse) data set, the cubic

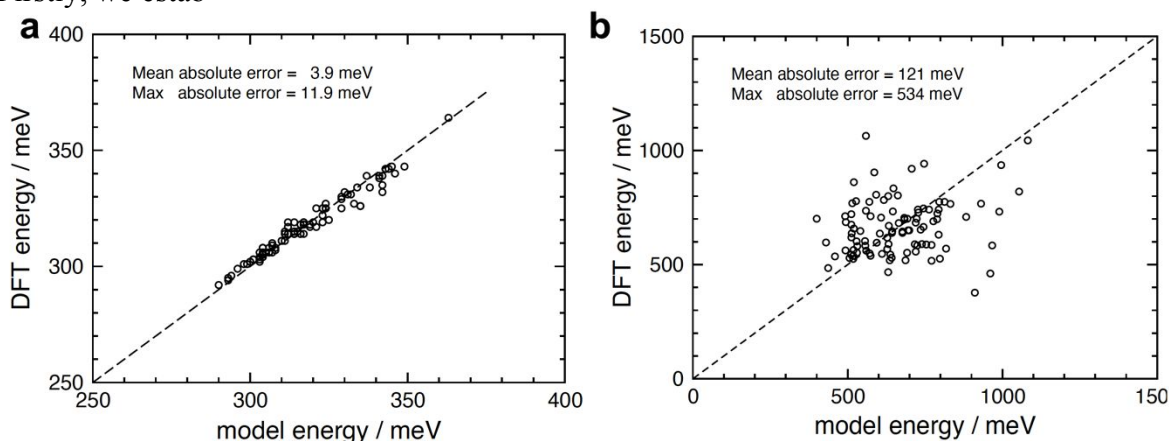
$$U = U_0 + k\left(\frac{a}{2} - l\right)^2 + 2k\left(\frac{a}{2} - l\right)^3 \quad (2)$$

with coefficients $k = 1996 \text{ meV/\AA}^2$ and $k_3 = -1934 \text{ meV/\AA}^3$ best approximates the data. Typical errors are of order a few meV. Combining both data sets produces a cubic fit with $k = 1979 \text{ meV/\AA}^2$ and $k_3 = -967 \text{ meV/\AA}^3$. Here the maximum absolute error is 5 meV, and a mean absolute error of 1.2 meV. By restricting the fit to data points with bond stretches of $\pm 0.1 \text{ \AA}$ maximum, the fit is improved to 0.34 meV maximum error and 0.22 meV mean, however this seems rather a tight restriction if looking to explain experimental bond length changes of the same magnitude.

Perturbed 1D chain The above protocol stretches all bond lengths uniformly which may not fully explore the energy landscape of infinite periodic 1D CsI chains. Two sets of 100 CASTEP calculations were therefore performed on 12 ion unit cells of a periodic chain (Figure 5S(a,b)). The periodic cell dimension was fixed at 45.02 \AA the periodicity of a (7,5) SWCNT, at which length only Γ -point calculations are required. Both non-periodic cell dimensions were set to 15 \AA . Ion positions were randomly perturbed by $\pm 0.1 \text{ \AA}$ to explore the energy landscape. Note however that this produces bond extensions of up to $\pm 0.4 \text{ \AA}$ when displacements reinforce and also that by fixing the overall length of the chain to 45.02 \AA , there are virtually zero contractions present in this test set.

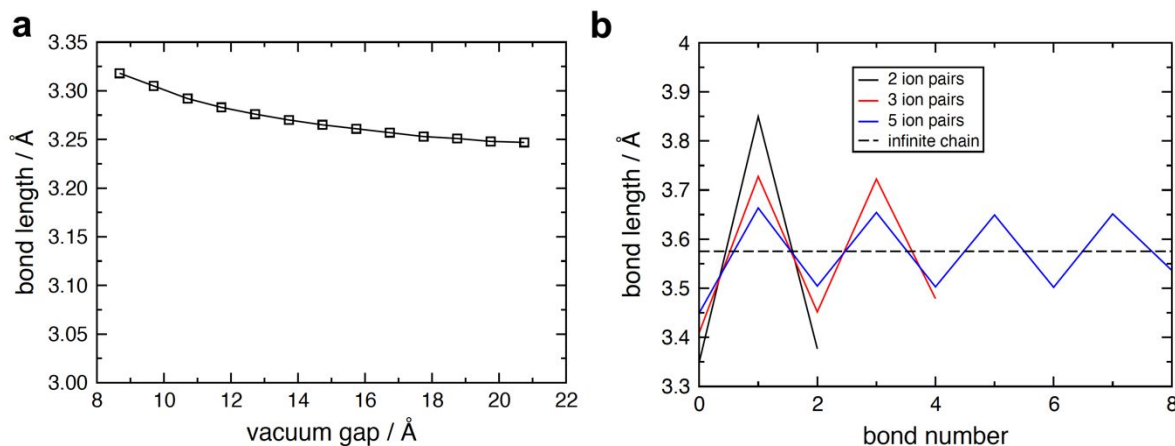
With the original (including the cubic term) fit to stretched unit cell data, the maximum absolute error between predicted and DFT energies is 11.9 meV (less than 0.1 meV error average per bond), and a mean absolute error of 3.9 meV. This is approximately twice as poor as for the smaller bond stretches in the fitting set, but is acceptable considering the majority of stretches are not expected to reach the large bond lengths which dominate the error. Refitting the model parameters based entirely on the configurations in this test set does not significantly improve the correlation - the mean absolute error reduces only to 1.8 meV.

Finite length chains In the context of mismatch strain, one method is to simulate a finite length of tube filling with a vacuum gap between periodic images.^{S4} The length of the finite wire increases to converge the inter-ion distance at its center to match that in an infinite periodic and unbroken chain. Firstly, we estab-



Supporting Figure S5 Correlation between fitted and DFT computed energies for two test sets. Each test set consists of 100 configurations of 12 Cs and I atoms in a 1d chain. Positions are perturbed randomly by up to the indicated magnitude along the chain direction: (a) Small perturbations ($\pm 0.1 \text{ \AA}$); (b) Large perturbations ($\pm 0.3 \text{ \AA}$).

lish the size of vacuum gap needed to converge the separation between an isolated pair of Cs and I atoms (20 Å was found to be sufficient) and then, using this size gap in all cases, compute the relaxed pair spacings in wires of 2, 3 and 5 ion pairs. Although the oscillation of bond lengths along increasingly longer chains dampens toward the infinite chain limit, significantly longer chains would be required to accurately resolve the differences of 0.1 Å seen in experiment.



Supporting Figure S6 Correlation between fitted and DFT computed energies for two test sets. Each test set consists of 100 configurations of 12 Cs and I atoms in a 1d chain. Positions are perturbed randomly by up to the indicated magnitude along the chain direction: (a) Relaxed ionic spacing for a single Cs-I pair as a function of vacuum gap; (b) Relaxed ionic spacings for isolated Cs-I chains with a vacuum gap.

Basic force field fitting in the absence of any tube Force field fitting was implemented using PotFit, created by Brommer and Gähler.^{S5} This program uses Born-Mayer type potentials, *i.e.* electrostatics created by the Wolf summation method with partial charges and the screening parameter κ treated as fitting parameters. This is truncated and shifted such that the electrostatic interaction is zero at the cut-off radius. Electrostatic interactions between ions are augmented with the usual Buckingham interactions, *i.e.*

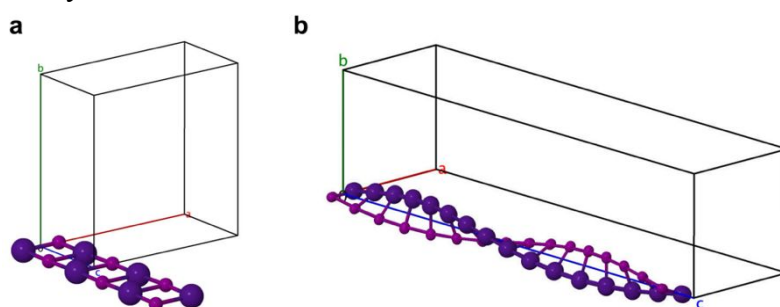
$$V(r) = \alpha \exp\left(\frac{r}{\beta}\right) - \gamma \left(\frac{\beta}{r}\right)^6 \quad (3)$$

PotFit uses the force matching approach. Here we ignore energies in the fit and attempt only to recover forces. Using the same DFT data set used earlier (100 configurations of 6 ion pairs in a linear chain with random perturbations on position of ± 0.1 Å) force matching was applied to produce the parameters shown as Set 1 in Table S1. Note that Mulliken charges extracted from the DFT output were ± 0.82 over the entire training set.

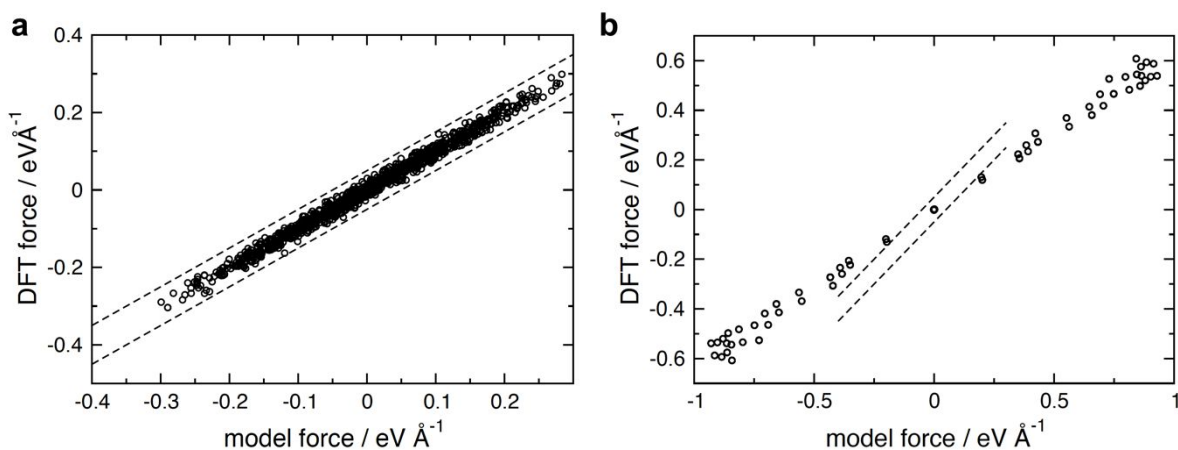
parameter	set 1	set 2
q_I	-0.934768	-0.842259
q_{Cs}	0.934768	0.842259
κ	0.047576	0.121038
$\alpha_{Cs,I}$	2675.878	5216.852
$\beta_{Cs,I}$	0.355732	0.357112
$\gamma_{Cs,I}$	3230.445	369.6561
$\alpha_{Cs,Cs}$	753.185	5087.37
$\beta_{Cs,Cs}$	0.38563	0.38628
$\gamma_{Cs,Cs}$	429.521	554.335
$\alpha_{I,I}$	2675.88	4923.349
$\beta_{I,I}$	0.37509	0.051441
$\gamma_{I,I}$	480.083	310.6189

Supporting Table S1 Born-Mayer potential parameters force-matched to DFT calculations on Cs-I chains in the absence of any CNT.

A test set was created from DFT calculations on helical nanowires. First a planar 2×1 wire (Fig. S7(a)) was relaxed to find the equilibrium Cs-I bond length (3.72 \AA) and spacing between dimers (3.71 \AA). Chains of dimers with this geometry were then twisted to create helices with a pitch of 6, 8, 10, 12, 14 and 16 (Fig. S7(b)) ion pairs. These were subsequently relaxed, with the forces calculated during the relaxation procedure stored to form the test set. Note that allowing the cell parameter to relax during these calculations resulted in collapse of the helix, however fixing the cell length to the appropriate integer multiple of the flat dimer spacing resulted in stable helices which did not unwind during relaxation. Forces produced from this model are compared to DFT forces (PBE functional, in Fig. S8). Correlation between the forces produced by parameter Set 1 and in these helical DFT calculations are shown in Fig. S8(a,b). Parameter Set 2 was produced by including the helical configurations in the training set. These parameters are listed in Table 1, and are dramatically altered. The optimized partial charges are now also much closer to the Mulliken charges produced by the PBE-DFT calculations.



Supporting Figure S7 Trial Ribbon and schematic twisted test model sets. Ribbon and example twisted configuration used in DFT calculations to create a helical data set: (a) Relaxed ribbon; (b) 16 ion pair helix, like charges on the same side of the 2×1 chain.



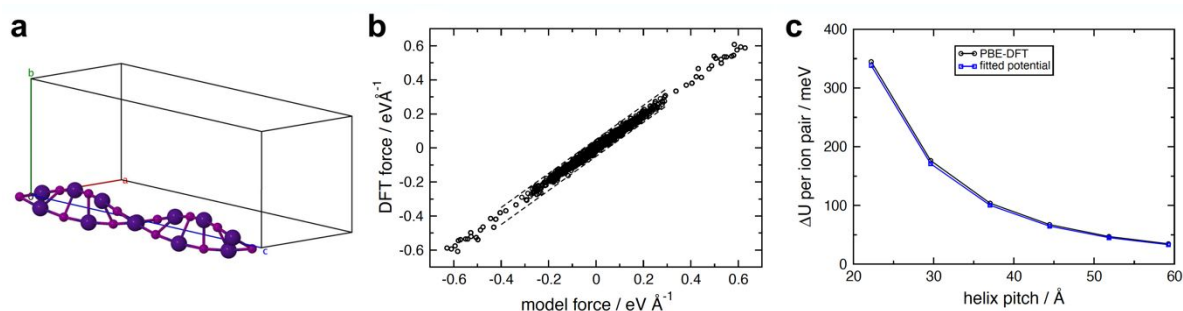
Supporting Figure S8 Correlation between fitted and DFT computed forces for the first Cs-I parameter set. Dashed lines denote force errors of $\pm 0.05 \text{ eV \AA}^{-1}$ - a typical tolerance used in geometry relaxation: (a) training set of 1D perturbed chains; (b) Test set of helical wires.

Alternating dipole helices Lower energy helical configurations can be created by alternating the direction of the Cs-I dipole in as shown in Fig. S9(a). Configurations with the same pitches used above were created, swapping the dipole direction of every second ion pair. This represents an ‘unseen’ test set for model potential parameter Set 2 (Fig. S9(b)). The twisting energy from the model is shown to be in excellent agreement with DFT in Fig. S9(c).

2×2 CsI nanowires The transferability of the current model was further tested with a 300K *ab initio* molecular dynamics simulation of 8 ion pairs arranged as two ion pairs in a 2×2 cross section nanowire. Dynamics were simulated for 1.6 ps and configurations extracted every 100 time steps. With this modified training data included the unfitted forces show some significant errors. Refitting to create potential set 3 involved:

- (i) Switching I-I and Cs-Cs interactions to Lennard-Jones potentials.
- (ii) Refitting the Cs-I Buckingham interactions
- (iii) Increasing the cutoff for Cs-I interactions to 15 \AA , and for like interactions to 10 \AA .

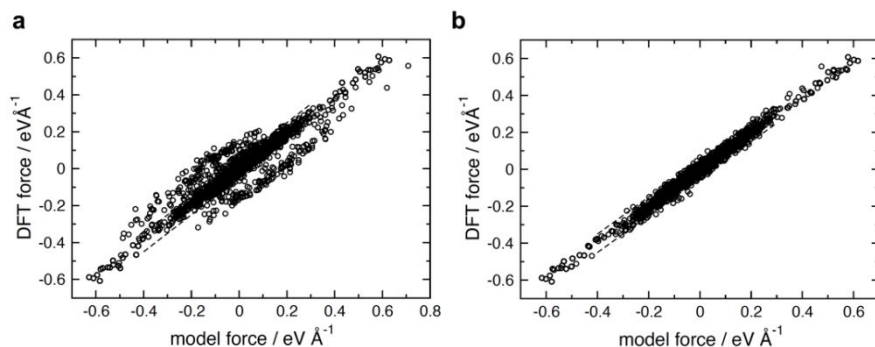
The first change was motivated by the observation that the fitted Buckingham interactions for like atoms were unconstrained at large radii by the fitting set and were diverging. The attractive part of the Cs-I Buckingham interaction was constrained to zero.



Supporting Figure S9 Energy change in twisting 2×1 wire of alternating dipoles into a varying pitch helix (see Fig. 4(a), main article): (a) Unit cell of alternating dipole helix with 12 ion pairs; (b). fitted vs DFT forces when using helical data within the training set; (c) Energy change in twisting 2×1 wire of alternating dipoles into a varying pitch helix. Results for both PBE-DFT and the fitted potential (parameter set 2) are shown. Energies relative are relative to an untwisted wire of infinite pitch.

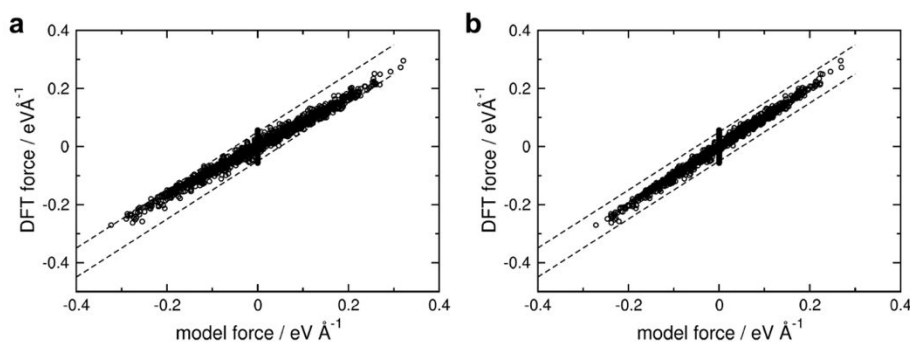
parameter	set 3
q_I	-0.854431
q_{Cs}	0.854431
κ	0.141208
$\alpha_{Cs,I}$	4745.79
$\beta_{Cs,I}$	0.36036
$\gamma_{Cs,I}$	0.00000
$\epsilon_{Cs,Cs}$	0.14742
$\sigma_{Cs,Cs}$	3.66345
$\epsilon_{I,I}$	0.12146
$\sigma_{I,I}$	3.30063

Supporting Table S2 Revised potential parameters force-matched to DFT calculations on Cs-I chains in the absence of any CNT.



Supporting Figure S10 | DFT vs model forces for data set including molecular dynamics snapshots of 8 ion pairs in a 2x2 cross section nanowire a. DFT vs model forces for data set including molecular dynamics snapshots of 8 ion pairs arranged as two ion pairs in a 2x2 cross section nanowire. Dashed lines denote force errors of $\pm 0.05 \text{ eV } \text{\AA}^{-1}$ - a typical tolerance used in geometry relaxation.

Perturbed 1D CsI chain inside a (7,5) SWCNT A set of DFT calculations was performed on the same 1D chain with random perturbations of ($\pm 0.1 \text{ \AA}$) as above (no off-axis perturbations) enclosed within a (7,5) CNT. As the model parameter set 2 is known to fit this system accurately without the CNT, a first test is to check model vs DFT forces, assessing the extent to which a model without wire-CNT interactions captures forces. One obvious feature of this modified DFT data set is that Mulliken charges are now consistently approximately +1.53 for Caesium and -0.37 for Iodine, substantially different from those outside of the tube. Correlation between model (parameter set 2) and DFT forces are shown with and without refitting of the atomic partial charges in Fig. S11(a) and (b) respectively.

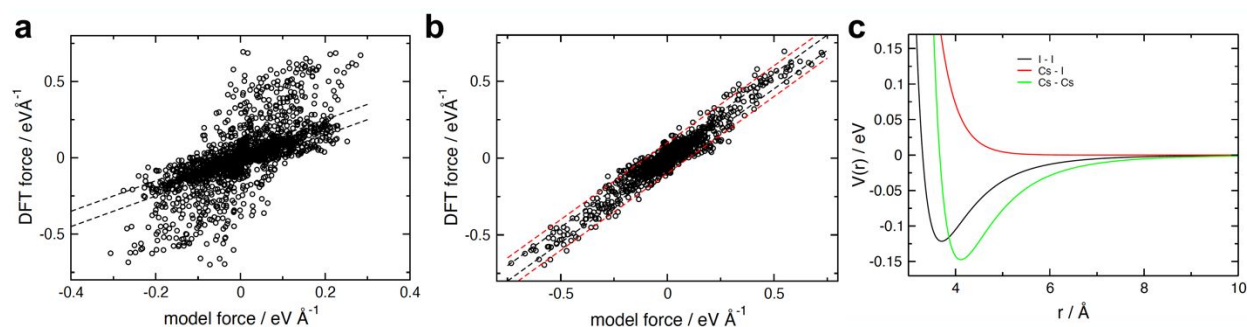


Supporting Figure S11 (a) DFT vs model forces for a data set of 100 12-ion configurations along the axis of a (7,5) CNT. The vertical feature at zero model forces corresponds to residual carbon-carbon interactions still present in the DFT-relaxed CNT structure. Refitted charges for Cs and I are ± 0.986483 with $\kappa = 0.16275$; (b) Essentially identical plots are produced with model set 3, where refitted charges are ± 0.957851 with $\kappa = 0.056660$.

Noting the charge asymmetry between Cs and I in the DFT calculations must results from charge transfer to the CNT, the average charge on C atoms was computed as -0.016 with a strong caution that these are only printed to a precision of 0.01 in CASTEP output. No improvement in fit could

be obtained using this as a fixed carbon charge whilst re-optimising the Cs and I charges, and if allowing the carbon charge to vary it relaxed back to zero.

CNT-ion interactions An additional 100 configurations were generated in which off-axis perturbations of $\pm 0.6 \text{ \AA}$ were also applied. Average partial charges in these configurations were not substantially different (1.57/0.38) to the on-axis case. Various functional forms for an ion-CNT interactions were tested, with a simple exponential repulsion resulting in the best fit amongst possibilities implemented in both PotFit and LAMMPS.^{S6} Note that this fitting kept the ion-ion interactions (and C-C *via* Tersoff) constant, and used only these 100 off-axis configurations. Including the on-axis configurations, which have zero or near-zero ion-carbon force produced a poorer fit. Note that PotFit cannot simultaneously use Tersoff and electrostatic interactions. To prevent the code from trying to fit the residual forces on carbon atoms due to C-C interactions, a dummy potential (*i.e.* Power Decay form) was included for C-C interactions in the fitting to mimic the Tersoff interactions.



Supporting Figure 12 DFT model forces for a data set of 100 12-ion configurations perturbed about the axis in a (7,5) CNT: (a) No CNT-ion interaction; (b) Fitted exponential repulsion (see also Table S3). Black dashed line denotes an error of $\pm 0.05 \text{ eV \AA}^{-1}$ and red dashed lines $\pm 0.1 \text{ eV \AA}^{-1}$; c. Fitted non-electrostatic component of ion-ion interactions as a function of ion separation or interaction.

The plots in Fig. S12(a,b) certainly indicate that the CNT-ion interaction is the most poorly represented at this level of model. Improved models incorporating charge transfer will be investigated in future. In the meantime, the extent to which useful progress can be made with the present model will be investigated. A particular warning should be given - the CNT-ion interactions are fitted to a single (7,5) nanotube only.

parameter	set 3
$\alpha_{C,I}$	9615.247
$\beta_{C,I}$	3.637456
$\alpha_{C,Cs}$	9698.85
$\beta_{C,Cs}$	4.17515

Supporting Table 3 Extended potential set 3 including CNT-ion interactions.

LAMMPS Simulations For each of the nanotubes listed in table 4, 1×1 , 2×1 and 2×2 cross section CsI crystals were simulated. Initial conditions were constructed as follows:

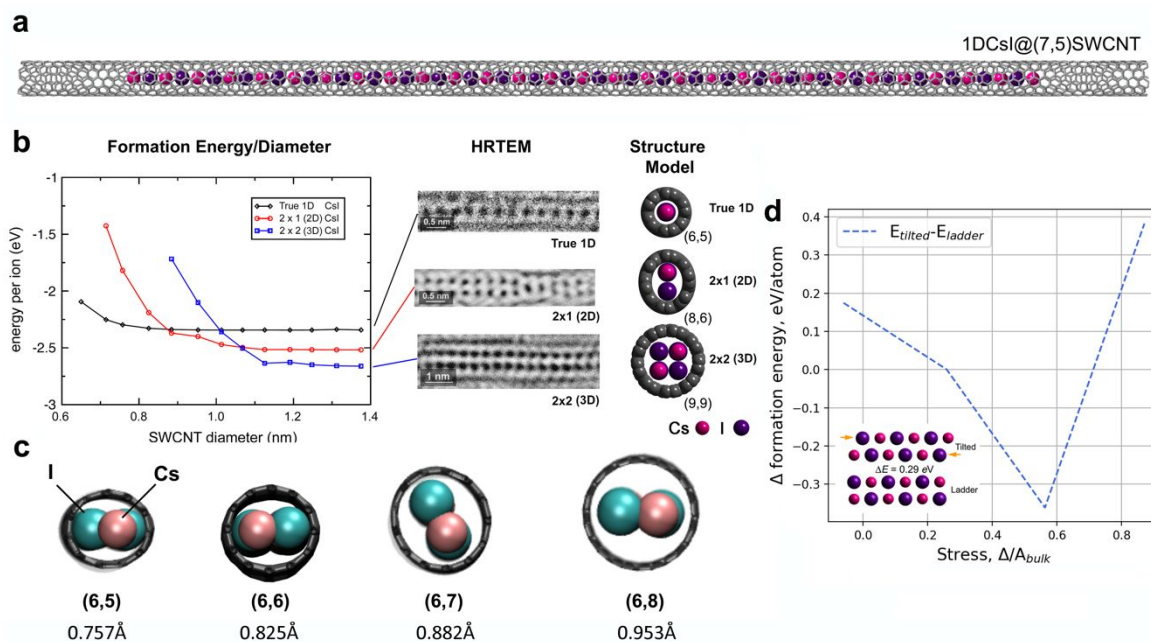
- (i) Sufficient periodic images of the CNT were used to reach a total length of $\sim 200 \text{ \AA}$.
- (ii) The CNT was partially filled with the CsI wire leaving 30 \AA between periodic images.
- (iii) Cell dimensions of 100 \AA were used in the non-periodic direction.

A sample initial geometry for a 1D CsI chain in a (7,5) SWCNT is shown in Fig. S13(a). Similar initial conditions were prepared with a 100 nm tube and the same vacuum gap for all the structures in Table S4. Each simulation was subjected to energy minimization, allowing the unit cell as well as the atomic positions to relax in the periodic direction. An early attempt to capture the relative energetics of ions in each of the three structures as a function of CNT diameter is shown in Fig. S13(b) and a refined and extensive version of this plot is presented in Fig. 4(b), main article, in which some calculated energies >0 eV for forbidden structures are included. These plots correspond to the energy/ion of the CsI wire and include interactions between Cs and I ions, and between these ions and the CNT walls. Including the carbon-carbon interaction energy is not straightforward as the number of C atoms per encapsulated ion is not constant with tube diameter. A further limitation of these data is that any distortion of the encapsulating CNT, and the resulting energy penalty, is not captured however we calculate the formation energy for undistorted and distorted SWCNTs in Figs. S13(b) to determine the relative stability of encapsulated 2×1 CsI wires with respect to CsI linear chains and, at higher diameter, with embedded 2×2 CsI wires (this relative stability is re-examined *in tandem* with Bader analysis in the next section). Experimental measurements however indicate that 2×1 CsI wires are realised at average diameters ($\bar{\varnothing}$) slightly narrower (*i.e.* ~ 0.88 nm or ~ 8.8 Å, Fig. 1(c), main article) than the 9 Å crossover suggested in Figs. S13(b) and 4(b) so are in reasonable agreement with our calculations. 2×2 CsI wires in small diameter tubes are probably less stable than Fig. 13(b) suggests.

Bader Analysis The charge distributions shifts in terms of outmost valence electrons and also formation energies of CsI linear chains, 2×1 CsI wires and embedded 2×2 CsI wires were also examined by Bader analysis (Ref. 37, main article) and Table 1 and Fig. 4(c) in the main article.

nanotube	diameter / Å
(7,2)	6.50 Å
(9,0)	7.15 Å
(6,5)	7.57 Å
(7,5)	8.18 Å
(6,6)	8.25 Å
(6,7)	8.82 Å
(10,2)	8.84 Å
(6,8)	9.53 Å
(12,0)	9.53 Å
(11,3)	10.14 Å
(11,4)	10.68 Å
(11,5)	11.26 Å
(15,0)	11.91 Å
(11,7)	12.48 Å
(11,8)	13.12 Å
(10,10)	13.75 Å

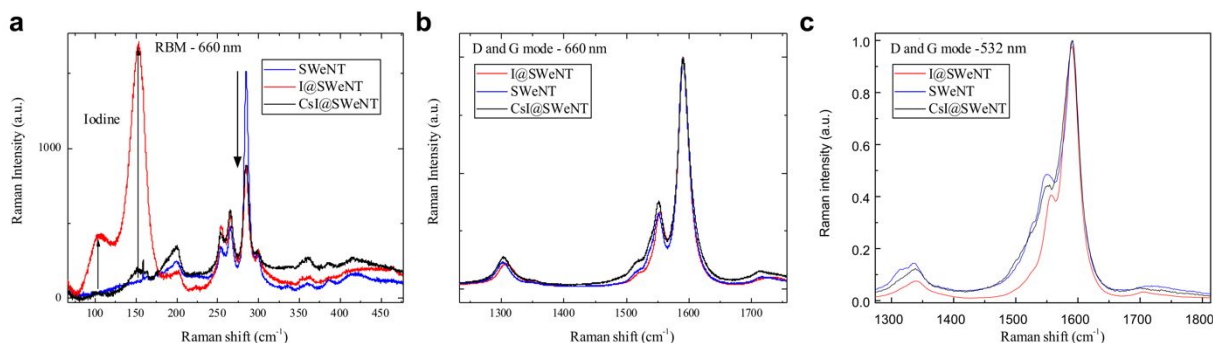
Supporting Table 4 Notional diameters of nanotubes simulated in this study.



Supporting Figure S13 Simulation geometries, formation energies of 1×1 , 2×1 and 2×2 CsI wires in undistorted/distorting SWCNTs and tilting energy with stress: (a) Initial simulation geometry of 1×1 wire in a 0.818 nm diameter (7,5) CNT; (b) Embedding energy per ion for CsI wires with potential set 3 as a function of cross section and notional SWCNT diameter (see also Fig. 4(b), main article). Inset at right middle are three HRTEM images of representative SWCNT embedded microstructures with their corresponding microstructures indicated at far right. The theory prediction here revises down the minimum possible diameter for 2×2 CsI formation to ~ 1.12 nm vs the experimentally reported value of ~ 1.4 nm (Ref. 11, main article); (c) Oval distortion of narrow diameter CNTs by conformation, with indicated average diameter, when encapsulated 2×1 CsI wires. Zero distortion is evident by (12,0); (d) Difference in formation energy/atom vs stress for ‘tilted’ vs ‘ladder’ 2×1 CsI (*cf.* Fig. 4(c), main article).

FURTHER RAMAN MEASUREMENTS

Here we record Supporting Raman measurements recorded at 660 nm excitation in the RBM shift range (*i.e.* 0-500 cm^{-1} , Fig. S14(a)) and also at 532 nm and 660 nm excitation (*i.e.* 1275-1825 cm^{-1} , Figs. S14(b) and S14(c), respectively) in the D and G band range for pure SWeNT SWCNTs, Iodine filled and CsI filled SWeNT SWCNTs.

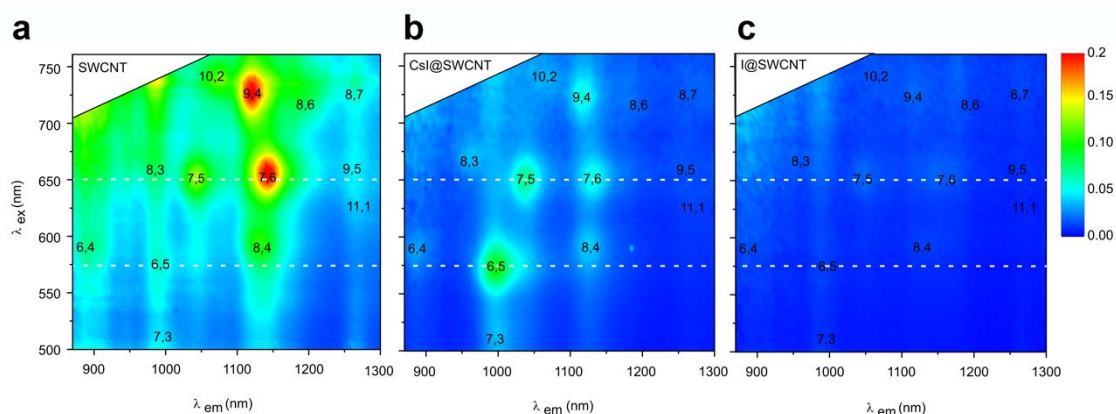


Supporting Figure S14 Resonant Raman spectroscopy obtained in the RBM region and D and G region at 660 nm and 532 nm: (a) Resonant Raman radial breathing modes (RBM) spectra for Iodine-filled, as-supplied SWeNT and CsI-filled SWCNTs, respectively, obtained at 660 nm

excitation (see also Fig. 6(a), main article for excitation at 532 nm). In this plot, the iodine I_3^- trimer resonances at $\sim 110\text{ cm}^{-1}$ and 151 cm^{-1} are clearly visible, whereas the $-Cs-I-Cs-I-$ 1D phonon resonance at 196 cm^{-1} (*cf.* Fig. 6(a), main article) is suppressed. Additionally, for both the CsI and Iodine filled SWCNT samples, the RBM resonance at 286 cm^{-1} is suppressed relative to the unfilled SWCNTs as indicated by the black downwards arrow. (b) and (c) D and G band spectra obtained at 660 nm excitation and 532 nm excitation.

ADDITIONAL PHOTOLUMINECSCENCE DATA

The plots in Figs. S15(a-c) present the full range of PL measurements that were made on empty SWCNTs, CsI filled SWCNTs and iodine filled SWCNTs. Figs. S15(a) and (b) are reproduced in Fig. 6(d), main article. The full range of PL emissions for the dispersed SWeNT sample can be seen in Fig. S15(a), significant PL emissions can still be seen for (6,5), (7,5), (8,4), (7,6) and (9,4) SWCNTs in Fig S15(b), for the iodine filled SWCNTs, all the PL emissions are suppressed.



Supporting Figure S15 Full 2D PL plots for unfilled SWCNTs, CsI-filled SWCNTs and Iodine-filled SWCNTs: (a) PL plot of empty SWeNT SWCNTs; (b) CsI-filled SWeNT SWCNTs; (c) iodine-filled SWeNT SWCNTs. The relative populations of (n,m) SWCNTs are discernible in the 2D plot for the empty SWCNTs (left) whereas the CsI-filled SWCNTs retain strong (6,5) and blue-shifted (7,5) and (7,6) emissions, respectively (middle plot). For the iodine-filled SWCNTs (right plot), nearly all the $E_{s,1}^s$ emissions SWCNTs are quenched (*cf.* Fig. 6(d), main article).

Supporting References

- S1. Rasband, W.S., ImageJ, U. S. National Institutes of Health, Bethesda, Maryland, USA. <https://imagej.nih.gov/ij/>, 1997-2018 (22/11/2021).
- S2. http://www.dmscripting.com/hrtem_filter.html (22/11/2021).
- S3. Barzilai, J., Borwein, J. M. 2-Point Step Size Gradient Methods, *IMA J. Numer. Anal.*, **8**, 141-148 (1988).
- S4. Brommer, P., Quigley, D. Automated Effective Band Structures for Defective and Mismatched Supercells. *J. Phys. Cond. Matter.*, **26**, 485501 (2014).
- S5. Brommer, P., Gähler, F. Potfit: Effective Potentials from ab Initio Data. *Modelling Simul. Mater. Sci. Eng.* **15**, 295–304 (2007).
- S6. LAMMPS Molecular Dynamics Simulator <https://lammps.sandia.gov> (22/11/2021).